Nucleation Curves of Model Natural Gas Hydrates on a Quasi-Free Water Droplet

Nobuo Maeda
CSIRO Manufacturing Flagship, Ian Wark Laboratory, Clayton, VIC 3168, Australia

DOI 10.1002/aic.14898
Published online June 8, 2015 in Wiley Online Library (wileyonlinelibrary.com)

Heterogeneous nucleation probability distributions of gas hydrates on a water droplet that was supported by inert and immiscible perfluorocarbon oil, perfluorodecalin is studied. The guest gas used was a mixture of 90 mol % methane and 10 mol % propane. The probability distribution was measured using a high pressure automated lag time apparatus under the guest gas pressure range of 6.7–12.5 MPa and the cooling rate range of 0.002–0.02 K/s. Nucleation curves were derived for unit area of water surface. The nucleation rate per unit area of water surface that was contained in a glass sample cell, which differed significantly from that on a quasi-free water droplet, is also derived. It is concluded that the nucleation curves in the presence of a solid wall should be normalized to the unit length of the three-phase line at which water, guest gas, and the solid wall meet. © 2015 American Institute of Chemical Engineers *AIChE J*, 61: 2611–2617, 2015

Keywords: nucleation, hydrates, nucleation curve, nucleation rate, gas hydrate, natural gas

Introduction

Clathrate hydrates or gas hydrates are crystalline solids that form when typically nonpolar guest molecules are enclosed in a hydrogen-bonded network of water molecules under conditions of low temperatures and high pressures.[1] Gas hydrates offer promising potentials in gas storage,[2,3] carbon sequestration,[4,5] and water desalination.[6,7] Natural methane hydrates in sediments could become a large potential energy source of future.[3] Conversely, formation of gas hydrates in natural gas pipelines pose serious risks to flow assurance.[1]

Gas hydrates are, by definition, multicomponent systems. The solubility of typically nonpolar guests in host water is so low that gas hydrates can only form at the water–gas interface where the concentration of the guest is the highest.[1] As such, effort when the formation of gas hydrates is desired has been primarily directed to increasing of the effective interfacial area by means of vigorous stirring, use of fine ice powder,[8] nanobubbles,[9] or dry water.[10] What is not known, however, is the heterogeneous nucleation rate per unit surface area of water at a given subcooling, ΔT, or the nucleation curve.

We previously measured a large number of induction time distributions for water that is contained in a glass sample cell (aka "boat") using high pressure automated lag time apparatus (HP-ALTA) MkI, and derived an empirical equation that relates the most probable induction time (the inverse of nucleation rates) as a function of subcooling.[11] However, complication arose when we attempted to convert the derived empirical equation to a nucleation curve. It was experimentally observed that the nucleation of gas hydrate films always originated at the three-phase-line where the glass wall, water, and the gas met.[12,13] Consequently, it remained unclear as to whether the experimentally measured heterogeneous nucleation probability distributions were proportional to the water–gas interfacial area or to the length of the three-phase-line.

HP-ALTA MkII, in contrast, measures the nucleation probability of gas hydrates on a single quiescent (unstirred) quasi-free water droplet that is supported by chemically inert and immiscible perfluorocarbon liquid oil, perfluorodecalin. It was observed that the maximum achievable subcoolings were significantly greater for such a quasi-free water droplet than for the water contained in a glass sample cell in an HP-ALTA MkI.[14] Even though HP-ALTA MkII has some instrumental limitations compared to HP-ALTA MkI (e.g., the range of cooling rate accessible is smaller, the deeper subcoolings required for nucleation significantly reduces the window of measurements before ice formation occurs), there are a few clear advantages. First, the surface area that is relevant to heterogeneous nucleation can be estimated with reasonable accuracy. Second, there is no need to estimate the effect of solid glass walls.

Here, we measured the nucleation rate of model natural gas hydrate (90 mol % methane and 10 mol % propane; we refer to as C1/C3 mixed gas hereafter) on a quasi-free water droplet using HP-ALTA MkII. We then derived nucleation curves from the data.

Materials and Methods

The descriptions of the HP-ALTA MkII instrument and the methods of preparations of quasi-free water droplet samples are documented elsewhere.[15] About 60 μL of water purified by a Millipore unit was placed on top of about 300 μL of perfluorodecalin, which is denser than water.[16] Both water and

Correspondence concerning this article should be addressed to N. Maeda at Nobuo.Maeda@csiro.au.

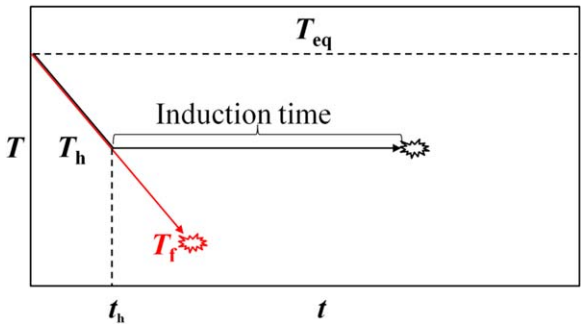

Figure 1. Schematic of cooling profiles in an HP-ATLA.

Two modes of measurements were used; the linear cooling ramp runs for the measurements of maximum achievable subcooling distributions (red) and induction time distribution runs (black). Here, the term "induction time" is defined as the time a sample remained subcooled at T_h, prior to eventual gas hydrate formation ($t > t_h$). When the time taken for the sample to reach T_h is included, the total time is referred to as "total time spent subcooled." [Color figure can be viewed in the online issue, which is available at wileyonlinelibrary.com.]

perfluorodecalin gradually evaporate during the course of the measurements, so these volumes provide the upper bound. Surface tension of perfluorodecalin is 19 mN/m which is much lower than that of water (72 mN/m).[17] So, a thin layer of perfluorodecalin climbed on top of the water droplet and covered most, if not all, of the surface of the water droplet.

We note that the shape of the water droplet was not exactly spherical. Rather, it appeared more ellipsoidal (flatter than spherical; the ratio of the horizontal axis to the vertical axis was about 4 to 3), presumably due to gravity. We did not analyze the shape of each water droplet. For calculations of the surface area, we assumed a spherical shape. Then, a sphere of 60 μL of water has the radius of about 2.4 mm and the surface area of about 74 mm^2.

The solubility of methane or propane in perfluorodecalin is not available in the literature. However, the solubility of hydrocarbon gases in fluorocarbons is generally much greater than that in water (by a factor of at least >10; for FC-104, for example, the solubility of methane is 22 times higher than that of water and the solubility of ethane is 50 times higher).[16,18] Given the much higher solubility of hydrocarbon gases in fluorocarbons than in water, we assume that the availability of guest gases is not a limiting factor that could hinder the nucleation of gas hydrates at the surface of the quasi-free water droplet.

Like HP-ALTA MkI, HP-ALTA MkII can be operated using one of the two modes; (1) keep cooling the sample at a constant cooling rate until gas hydrate formation or ice formation is forcibly induced at the formation temperature, T_f, or (2) cool the sample at a constant cooling rate to a predetermined target holding temperature, T_h, and hold the temperature of the sample constant at T_h thereafter. We show the temperature profiles of the two modes schematically in Figure 1. In either case, each measurement was isobaric and the guest gas pressure was selected in the range between 6.7 and 12.5 MPa. The heating conditions of 310 K for 200 s were used after each cooling ramp or induction time measurement, to avoid the so-called memory effect.

In our earlier study using HP-ALTA MkI, we found that induction times could be very long, especially at shallow subcoolings.[11] Consequently, we had to set an arbitrary cutoff maximum waiting time of 15,000 s for the second mode of operation.[11] In the current study, we also used the maximum waiting time of 15,000 s for the second mode of operation.

Results

Figure 2 shows an example chronological histogram ("Manhattan"[19]) of lag times during linear cooling ramps (a), the corresponding maximum achievable subcooling distribution or survival curve (b), and an example induction time distribution at a constant subcooling (c). The example maximum achievable subcooling distribution [(a) and (b)] was measured

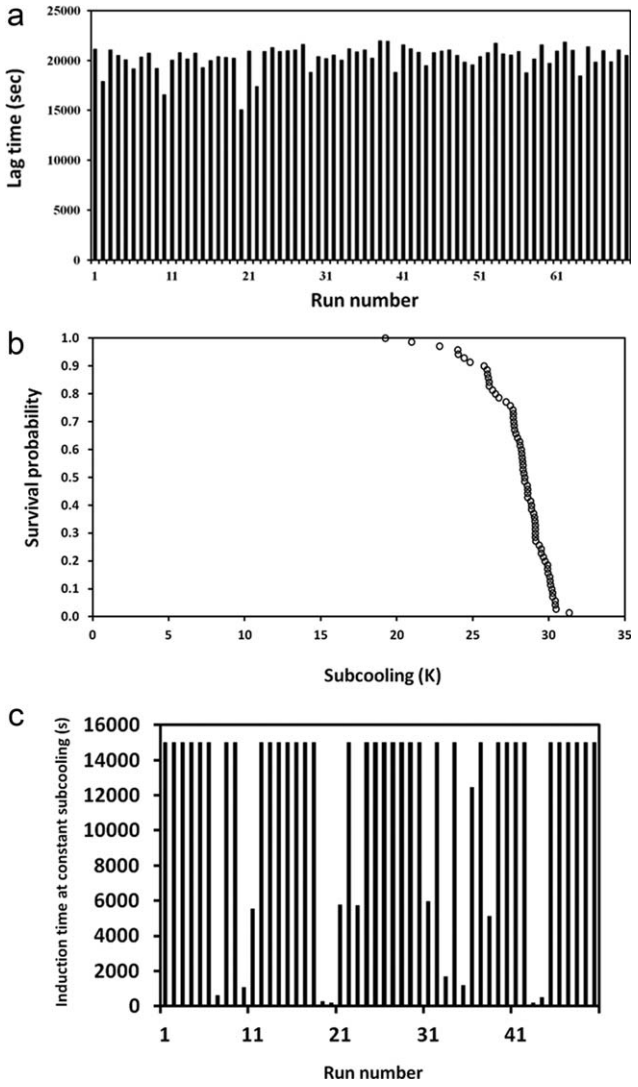

Figure 2. A typical chronological historgram of lag times during linear cooling ramps (a), the corresponding survival curve (maximum achievable subcooling distribution) (b), and an induction time distribution at a constant subcooling (c).

The example chronological historgram of lag times and the corresponding survival curve were measured at a cooling rate of 0.002 K/s and under 12.0 MPa of C1/C3 mixed gas. The induction time distribution was measured at the constant temperature of 270 K and under 10.0 MPa of C1/C3 mixed gas. Many runs reached the maximum waiting time of 15,000 s.

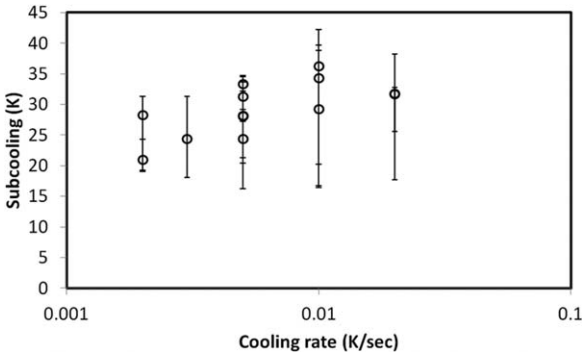

Figure 3. Summary of cooling rate dependence of the maximum achievable subcooling distributions.

The "error bars" show the whole range of the survival curves. It can be seen that the maximum achievable subcoolings slightly increased with the cooling rate, as expected.

at a cooling rate of 0.002 K/s and under 12.0 MPa of C1/C3 mixed gas. The example induction time distribution (c) was measured at the constant temperature of 270 K and under 10.0 MPa of C1/C3 mixed gas. As can be seen, many runs reached the maximum waiting time of 15,000 s.

We previously found that deeper subcoolings were required for the formation of C1/C3 mixed gas hydrates on quasi-free water droplets in HP-ALTA MkII than for a water sample contained in a glass sample cell (aka a "boat") in HP-ALTA MkI.[14] In our earlier study, we kept the selection of T_h to at or above 273 K to avoid ice formation.[11] Even though our another previous study showed that ice did not form in a quasi-free water droplet above 264 K in the pressure range of the current study,[14] we were reluctant to set T_h lower than 270 K. Because of the typically deeper subcoolings required, the induction times at a T_h at 270 K or above were longer and more runs reached the maximum waiting time of 15,000 s than in the previous study using HP-ALTA MkI.

Figure 3 shows a summary of the cooling rate dependence of the maximum achievable subcooling distributions (the first mode of operation). Our earlier study using HP-ALTA MkI showed that both the maximum T_f and the median T_f measured at various guest gas pressures were largely parallel to the phase boundary, $T_{eq}(P)$.[20] Then, the data measured at different guest gas pressures may be compared by converting the absolute gas hydrate formation temperature, T_f, to the subcooling, ΔT, via $\Delta T \equiv T_{eq} - T_f$. Here, the "stochasticity bars" show the whole range of the maximum achievable subcooling distributions, as previously explained.[20] It can be seen that the maximum achievable subcoolings slightly increased with increasing cooling rate, as expected.

As linear cooling ramps were used to vary the sample temperature, the total time a sample has spent in the subcooling region of the phase diagram prior to its eventual gas hydrate formation can be calculated for both modes of operation. In Figure 4, we show the data from the two modes of operation together. Note that all the induction time runs (the black data points) above 15,000 s only provide the lower bound as the maximum waiting period of 15,000 s was reached. That many induction time runs at a constant T_h had reached the maximum waiting time of 15,000 s severely limited the utility of the second mode of operation. For this reason, we did not use these data for the analyses presented below. Nevertheless, they still possess some utility in showing that the results from the two modes of operation did not differ massively from each other. In contrast, all of the linear cooling ramp runs resulted in the formation of either gas hydrate or ice. Our earlier results with pressurized nitrogen gas showed that ice did not form in a quasi-free water droplet above 264 K and that the medians of ice formation were in the range 259.5–261.5 K for the pressure range of the current study.[14]

Analyses and Discussion

Before we get into the details of the discussion of our results, it is pertinent to stop and ask; what does an HP-ALTA measure? An HP-ALTA measures the gas hydrate formation temperature distribution, or a combined effect of nucleation and growth of gas hydrates. Critical nuclei are simply too small to be detected by HP-ALTA, or by any other instrument for that matter. The question, then, is how much systematic error can arise from the delay in the detection of the nucleation events.

We had previously showed that, for MkI, the growth rate of C1/C3 mixed gas hydrate films on water surface increased with subcooling.[13] At a subcooling of 20 K, for example, the growth rate of the film ranged between 0.1 and 0.7 mm/s.[13] If we assume that a similar growth rate holds for gas hydrate films on the surface of a quasi-free water droplet, we can estimate the amount of potential detection delay in HP-ALTA MkII. The detection light beam passes through the droplet vertically. Gas hydrate formation can be detected when the growth reaches the North Pole or the South Pole of the droplet. Thus, the longest delay occurs when the nucleation originates at a point along the equator. It will take at most 38 s for gas hydrate films to travel from the equator to a pole of a typically sized (radius $\approx$ 2.4 mm) quasi-free water droplet. For the typical cooling rate of 0.005 K/s used for MkII, this lag will cause a systematic error of at most 0.2 K. The systematic error will be smaller when a slower cooling rate is used and/or when

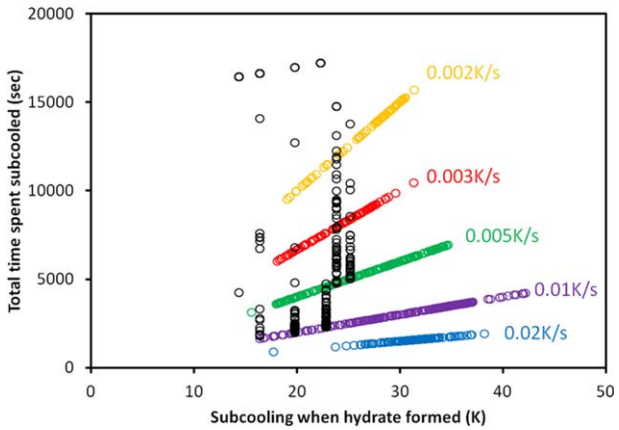

Figure 4. Total time spent subcooled prior to eventual nucleation of C1/C3 mixed gas hydrates is shown as a function of subcooling at which the said eventual nucleation took place.

The black data points are from the induction time distribution runs and the colored data points are from the linear cooling ramp runs. All the black data points above 15,000 s (many are overlapping with each other) only provide the lower bound as the maximum waiting period of 15,000 s was reached. [Color figure can be viewed in the online issue, which is available at wileyonlinelibrary.com.]

nucleation occurs at deeper subcoolings for which the film growth rate is faster. As our data showed that the use of a faster cooling rate typically led to deeper subcoolings achievable, these two factors more or less cancel out. In other words, the systematic error in the maximum achievable subcoolings due to the possible lag in detection in an HP-ALTA MkII is at most 0.2 K, or about 1% of the maximum achievable subcooling values. We note that the estimated systematic error in this study is significantly smaller than that in an HP-ALTA MkI of at most 1 K, for which the cooling rate was faster and the maximum achievable subcoolings were smaller.[21] We may assume, then, that the gas hydrate formation temperature distributions measured by an HP-ALTA MkII closely match the nucleation probability distributions (i.e., the nucleation probability increases from 0 to 1 over the range of a survival curve).

We also note at this stage that homogeneous nucleation is a limiting case of heterogeneous nucleation for which the contact angle, θ, is 180°. It follows that the nucleation barrier for heterogeneous nucleation is proportional to that of homogeneous nucleation; $\Delta G_{\text{hetero}}/\Delta G_{\text{homo}} = (2+\cos\theta)(1-\cos\theta)^2/4$.[22] The point is that the same functional form of nucleation curves holds for both homogeneous nucleation and heterogeneous nucleation, albeit with different prefactors.

Below, we first describe the method of analysis used in the study and then apply the method to our data.

Induction time at a constant subcooling ΔT

We assume that the survival curve at a constant subcooling temperature $F(t)$ represents the survival probability that diminishes with time, t. We define the nucleation probability density at time t as $p(t)$.

The nucleation probability between t and $t+dt$ then becomes $p(t)dt$.

Now, the survival probability at $t+dt$ is the survival probability at t multiplied by the probability that nucleation does not occur in the subsequent duration dt, which is $[1-p(t)dt]$. Thus

$$F(t+dt)=F(t)\cdot[1-p(t)dt] \tag{1}$$

Then

$$[F(t+dt)-F(t)]/F(t)=-p(t)dt \tag{2}$$

It follows that

$$d(\ln F(t))/dt=-p(t) \tag{3}$$

At each moment, t, the nucleation probability density, p, is given by the negative of the derivative of $\ln F$ with respect to t at that t.

By solving the differential equation

$$F(t)=\exp[-p(t)\cdot t] \tag{4}$$

If we define the most probable survival time (induction time), $<t>$, as the time when 50% of the samples are frozen, then

$$<t> = \ln 2/p(t) \approx 0.7/p(t) \tag{5}$$

This can be verified by substituting $t=\ln 2/p(t)$ into $F(t)=\exp[-p(t)\bullet t]$, which yields $F(t)=2^{-1}=0.5$.

Now, the nucleation rate, k, is defined as $k \equiv <t>^{-1}$. Then

$$k=p(t)/\ln 2 \approx p(t)/0.7 \tag{6}$$

The nucleation rate is constant at a given subcooling, regardless of the sample history. The nucleation rate at a given subcooling can be calculated from the negative derivative of the natural logarithm of the constant subcooling survival curve (if we can measure one).

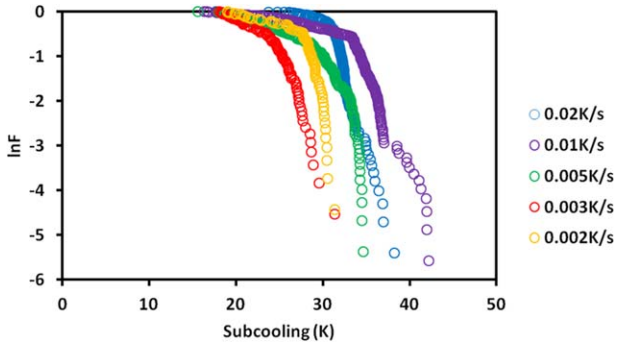

Figure 5. All the survival curves, measured at various guest gas pressures but using the same cooling rate, were combined to produce a single survival curve, $F_{\Delta T}$, for each cooling rate.

Here, the natural logarithm of the combined survival curve, $\ln F_{\Delta T}$, for each cooling rate is plotted against subcooling (K). [Color figure can be viewed in the online issue, which is available at wileyonlinelibrary.com.]

During a linear cooling ramp at a constant cooling rate of α

Using the same logic as the derivation of Eq. 1, the survival probability, $F_{\Delta T}(t)$, is

$$F_{\Delta T+d(\Delta T)}(t+dt)=F_{\Delta T}(t)\cdot[1-p_{\Delta T}(t)dt] \tag{7}$$

This time ΔT is not constant and changes with t. In the duration dt, ΔT changes by αdt. At the same time, $F_{\Delta T}$ will change to $F_{\Delta T+\alpha dt}$. However, this may be approximated by the average of $F_{\Delta T}$ and $F_{\Delta T+\alpha dt}$. To the first approximation, we approximate $F_{\Delta T+\alpha dt}$ with $F_{\Delta T}$ here. Then

$$[F_{\Delta T}(t+dt)-F_{\Delta T}(t)]/F_{\Delta T}(t)=-p_{\Delta T}(t)dt \tag{8}$$

$$d(\ln F_{\Delta T}(t))/dt=-p_{\Delta T}(t) \tag{9}$$

At each moment, t, the nucleation probability density, $p_{\Delta T}(t)$, is given by the negative of the derivative of $\ln F_{\Delta T}$ with respect to t at that t and ΔT. As before

$$k=p_{\Delta T}(t)/\ln 2 \approx p_{\Delta T}(t)/0.7 \tag{10}$$

What these analyses mean is that the nucleation probability at a given moment (and subcooling) depends only on the local slope of the natural logarithm of the survival curve at that moment (and subcooling), and does not depend on the previous sample history up to that moment (i.e., assume the Markov property).

Analyses of the data

Figure 5 shows the natural logarithm of the survival curves, $\ln F_{\Delta T}$, as a function of subcooling, ΔT, for each cooling rate used in the study. $\ln F_{\Delta T}$ as a function of time can then be readily obtained by dividing the subcooling with the corresponding cooling rate (the shape of each curve remains the same as that shown in Figure 5 but the scale of the x axis becomes different for each curve).

There are several ways to calculate the local slope of $\ln F_{\Delta T}$ with respect to time. The most direct way would be to calculate the slope at each point using a moving average of an

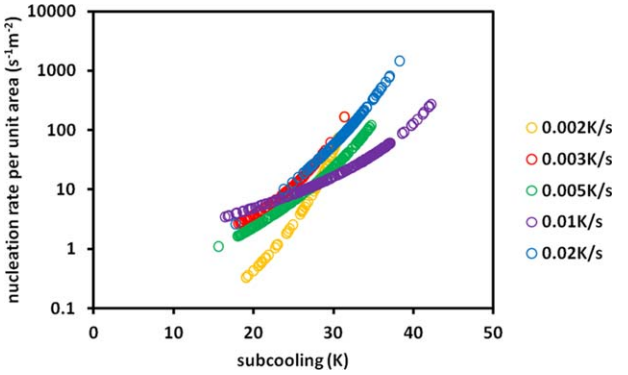

Figure 6. The negative of the slope of $\ln F_{\Delta T}$ with respect to time yields the nucleation probability density, p.

The nucleation rate is proportional to the probability density by a factor of ln2. The nucleation curves (the nucleation rate normalized for unit water surface area) are shown for each combined survival curve shown in Figure 5. The data for subcoolings greater than about 35 K are likely due to freezing of water (ice formation) and may not reflect the nucleation rate of gas hydrate. [Color figure can be viewed in the online issue, which is available at wileyonlinelibrary.com.]

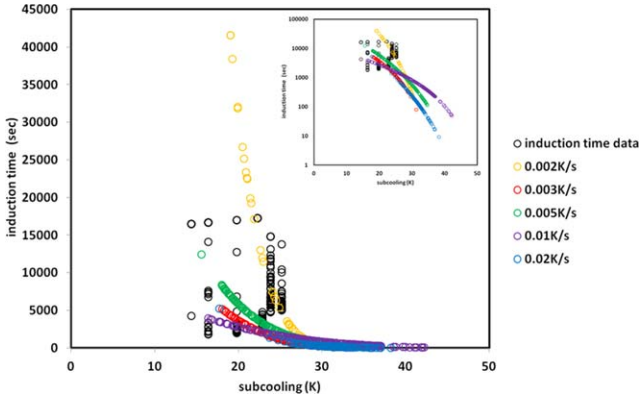

Figure 7. The nucleation curves shown in Figure 6 are used to calculate the most probable survival time, <t>, for the area of the quasi-free water droplet (74 mm^2).

The reconstructed nucleation curves are shown together with the data from the induction time distribution runs (the black data points in Figure 4). Both the linear and the semilog plots are shown. It can be seen that they are consistent with each other. [Color figure can be viewed in the online issue, which is available at wileyonlinelibrary.com.]

appropriate box size. However, as $F_{\Delta T}$ (and $\ln F_{\Delta T}$) monotonically decreases with time, here we fitted each curve with a simple power law and analytically differentiated the fitted curve with respect to t. The resulting nucleation curves, normalized for unit surface area, are shown in Figure 6. Here, we used 1 square meter as the unit area, following the MKS unit of systems. However, extrapolation of the nucleation rates to much larger or smaller scales must be carried out with caution. Interestingly, even though some variations were observed, no clear cooling rate dependence could be identified within the range studied, except perhaps that a slower cooling rate generally resulted in a lower nucleation rate. The nucleation rate is expected to become lower as the cooling rate is reduced if the survival curves measured using different cooling rates were identical. This is because the nucleation rate is proportional to the absolute value of the slope of $\ln F_{\Delta T}$ with respect to time (i.e., the absolute value of the slope becomes smaller as the time axis is being stretched).

It should be noted that parts of the nucleation curves at subcoolings deeper than 35 K are likely to be "contaminated" by ice nucleation events. Importantly, however, that does not affect the slope of $\ln F_{\Delta T}$, or the nucleation curves of gas hydrates, at subcoolings less than 35 K. The reason is that the survival probability at a shallow subcooling does not depend on the ultimate fate of the sample in the future (whether nucleation of gas hydrate takes place before ice freezing or not).

We can use Eq. 5 and the nucleation curves shown in Figure 6 to calculate the most probable survival time (induction time), <t>, for the surface area of the quasi-free water droplet (74 mm^2). The reconstructed curves are shown in Figure 7, together with the data from the induction time distribution runs (the black data points in Figure 4). It can be seen that the reconstructed nucleation curves overlap with the induction time distribution data from the second mode of operation.

Evaporation of the sample water

Corrections to account for the gradual evaporation of the water droplet, and the concomitant shrinkage of the surface area, are difficult to carry out. The rate of evaporation depends on the sample temperature and the saturation level of the space that surrounds the sample, and the sample temperature keeps changing (each cooling ramp continues until either a gas hydrate formation or ice formation is detected, the duration of which is different for each cooling ramp).

Rather than trying to quantify the extent of evaporation, we here merely point out that the nucleation rate is inversely proportional to the surface area. If the surface area had been monotonically and significantly shrinking during the course of an experiment, then one would expect a trend of progressively

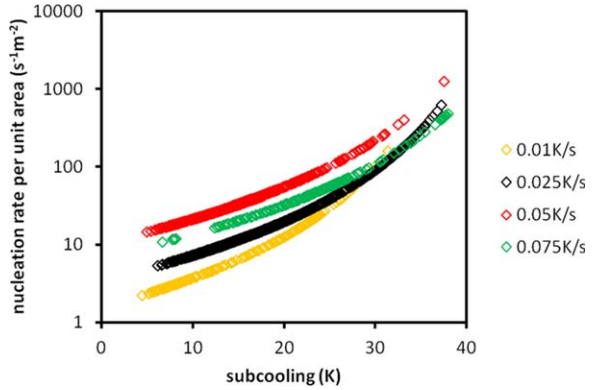

Figure 8. The nucleation curves (the nucleation rate per unit area) were calculated for the water sample contained in a glass sample cell (aka boat) of a HP-ALTA MkI, using the same procedure as that was used in the derivation of Figure 6.

The nucleation rate was normalized by the surface area of water that was exposed to the guest gas in the glass sample cell. The data for subcoolings greater than about 30 K are likely due to freezing of water (ice formation) and may not reflect the nucleation rate of gas hydrate. [Color figure can be viewed in the online issue, which is available at wileyonlinelibrary.com.]

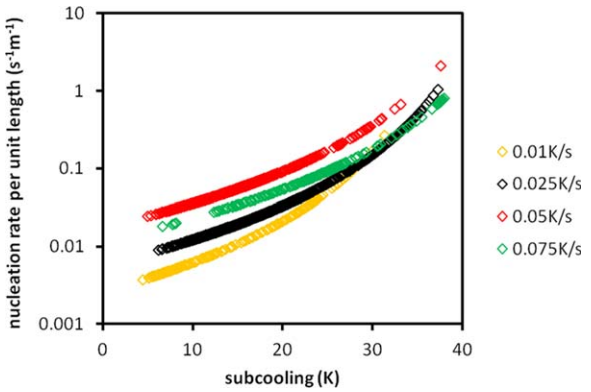

Figure 9. The nucleation curves were calculated for the water sample contained in a glass sample cell (aka boat) of a HP-ALTA MkI, only this time the nucleation rate was normalized by the unit length of the three-phase-line in the system (where the glass wall, sample water and guest gas met).

[Color figure can be viewed in the online issue, which is available at wileyonlinelibrary.com.]

deeper subcoolings (longer lag times) as the experiment progresses. However, we did not observe such trend from chronological histograms of lag times, such as the one shown in Figure 2a. Presumably, the shrinking surface area due to the gradual evaporation of the quasi-free water droplet during the timescale of an experiment was not significant.

Comparison to nucleation curves of water contained in a glass sample cell

Finally, we compare the current results to those obtained earlier using HP-ALTA MkI.[20] The dimensions of the glass sample cell (aka "boat") in MkI are such that the area of water–guest gas interface is approximately 132 mm^2 and that the length of the three-phase line is approximately 79 mm. We note that the length of the three-phase line is a macroscopic nominal length and does not account for any microscopic or submicroscopic surface roughness of the glass wall which might render the "real" length substantially longer. We can derive nucleation curves from the earlier data for each of the following two cases; first is to assume that the nucleation rate is proportional to the water–guest gas interfacial area and normalize the nucleation rate to the unit area; $J_{\text{water-guest}}$ (s^{-1} m^{-2}). The other is to assume that the nucleation rate is proportional to the length of the three-phase-line and normalize the nucleation rate to the unit length; $J_{\text{glass-water-guest}}$ (s^{-1} m^{-1}). The resulting nucleation curves are shown in Figures 8 and 9, respectively. Note that the data for subcoolings greater than about 30 K are likely due to ice freezing and may not reflect the nucleation rate of C1/C3 gas hydrates. As was the case with the quasi-free water droplet, no clear cooling rate dependence could be identified in the limited range studied except perhaps that slower cooling rates generally result in lower nucleation rates.

Comparison of Figures 6 and 8 shows that the nucleation rates at a given subcooling differ significantly. This discrepancy, together with the earlier experimental observation that nucleation always originated from the three-phase-line in HP-ALTA MkI, suggests that the nucleation rate per unit area of water surface is not an appropriate measure to use in the presence of a solid wall. After all, the presence of a solid wall is not at all accounted for in Figure 8. Instead, we propose that the nucleation rate per unit length of the three-phase-line (Figure 9) is the appropriate measure of the description of heterogeneous nucleation in the presence of a solid wall.

The basic idea is that the nucleation rate per unit length of the three-phase-line is a unique property for the solid in question. The greater of the total nucleation rate integrated over the whole length of the three-phase-line in a system or the total nucleation rate integrated over the whole surface area of water in the system determines the overall nucleation rate of the said system. For the case of a glass sample cell used in HP-ALTA MkI, the former exceeds the latter, and consequently any heterogeneous nucleation at the water–guest gas interface that is away from the solid walls will be superseded by the heterogeneous nucleation at the three-phase-line.

Conclusions

Nucleation curves were derived for heterogeneous nucleation of C1/C3 mixed gas hydrates on a quiescent (unstirred) quasi-free water droplet that is supported by perfluorodecalin with the following assumptions.

1. HP-ALTA measures heterogeneous nucleation probability distributions of gas hydrates. If, for example, only 1 in 100 cooling ramps resulted in a nucleation event at a certain subcooling then the nucleation probability at that subcooling is interpreted as 1%.

2. HP-ALTA cannot directly measure the formation of critical nuclei. It is assumed that given the typically deep subcoolings involved, nucleation will lead to rapid growth. The systematic error that can arise from this lag in detection due to the finite growth rates is at most 0.2 K.

3. The survival probability distributions measured at different guest gas pressures can be combined for the data measured using the same cooling rate if subcoolings are used as the representative measures. This assumption is supported by our previous studies which showed that both the medians of T_f and the minimum T_f measured at various guest gas pressures were largely parallel to the phase boundary, T_{eq}.

4. It is assumed that the availability of guest gas is not a limiting factor to gas hydrate nucleation. This assumption is supported by the fact that the solubility of hydrocarbon gases in perfluorocarbon oils is more than 10 higher than that in water.

5. The initial volume of 60 μL was used for the calculations of the surface area of the water droplet, and a spherical shape of the droplet was assumed, which gives the initial radius of 2.4 mm and the initial surface area of 7.4×10^{-5} m^2. These numbers provide the upper bound due to the gradual evaporation of the water droplet during the course of the measurements. The chronological histogram did not reveal any noticeable systemic increase in the subcooling with time.

With these assumptions, analyses were carried out to derive nucleation curves of the system. The results are summarized in Figure 6. We also reanalyzed the data for water sample that was contained in a glass sample cell. The results are summarized in Figures 8 and 9.

In light of the current results, and the reanalysis of the earlier results, we conclude that the nucleation rate per unit length of the three-phase line is the appropriate measure of the description of heterogeneous nucleation in the presence of a solid wall.

Acknowledgment

This work was supported by the Australian Research Council Future Fellowship (FT0991892) and CSIRO's Energy Flagship.

Literature Cited

1. Sloan ED, Koh CA. *Clathrate Hydrates of Natural Gases*, 3rd ed. Boca Raton, FL: CRC Press, 2008.
2. Ohgaki K, Inoue Y. A proposal for gas-storage on the ocean-floor using gas hydrates. *Kagaku Kogaku Ronbunshu*. 1991;17:1053–1055.
3. Englezos P. Clathrate hydrates. *Ind Eng Chem Res*. 1993;32:1251–1274.
4. Lee HH, Ahn SH, Nam BU, Kim BS, Lee GW, Moon D, Shin HJ, Han KW, Yoon JH. Thermodynamic stability, spectroscopic identification, and gas storage capacity of CO_2-CH_4-N_2 mixture gas hydrates: implications for landfill gas hydrates. *Environ Sci Technol*. 2012;46:4184–4190.
5. Lee Y, Lee S, Jin YK, Seo Y. 1-Propanol as a co-guest of gas hydrates and its potential role in gas storage and CO_2 sequestration. *Chem Eng J*. 2014;258:427–432.
6. Cha J-H, Seol Y. Increasing gas hydrate formation temperature for desalination of high salinity produced water with secondary guests. *ACS Sustain Chem Eng*. 2013;1:1218–1224.
7. Park KN, Hong SY, Lee JW, Kang KC, Lee YC, Ha MG, Lee JD. A new apparatus for seawater desalination by gas hydrate process and removal characteristics of dissolved minerals (Na^+, Mg^{2+}, Ca^{2+}, K^+, B^{3+}). *Desalination*. 2011;274:91–96.
8. Stern LA, Kirby SH, Durham WB. Peculiarities of methane clathrate hydrate formation and solid-state deformation, including possible superheating of water ice. *Science*. 1996;273:1843–1848.
9. Takahashi M, Kawamura T, Yamamoto Y, Ohnari H, Himuro S, Shakutsui H. Effect of shrinking microbubble on gas hydrate formation. *J Phys Chem B*. 2003;107:2171–2173.
10. Binks BP, Murakami R. Phase inversion of particle-stabilized materials from foams to dry water. *Nat Mater*. 2006;5:865–869.
11. Wu R, Kozielski KA, Hartley PG, May EF, Boxall J, Maeda N. Probability distributions of gas hydrate formation. *AIChE J*. 2013; 59:2640–2646.
12. Maeda N, Wells D, Becker NC, Hartley PG, Wilson PW, Haymet ADJ, Kozielski KA. Development of a high pressure automated lag time apparatus for experimental studies and statistical analyses of nucleation and growth of gas hydrates. *Rev Sci Instrum*. 2011;82: 065109.
13. Wu R, Kozielski KA, Hartley PG, May EF, Boxall J, Maeda N. Methane-propane mixed gas hydrate film growth on the surface of water and luvicap EG solutions. *Energy Fuels*. 2013;27:2548–2554.
14. Maeda N. Fuel gas hydrate formation probability distributions on quasi-free water droplets. *Energy Fuels*. 2015;29:137–142.
15. Maeda N. Measurements of gas hydrate formation probability distributions on a quasi-free water droplet. *Rev Sci Instrum*. 2014;85: 065115.
16. Lide DR. *CRC Handbook of Chemistry and Physics*, 95th ed. Boca Raton, FL: CRC Press, 2015.
17. Littlejohn GR, Love J. A simple method for imaging Arabidopsis leaves using perfluorodecalin as an infiltrative imaging medium. *J Vis Exp*. 2012;59, e3394, doi:10.3791/3394.
18. *Solubility of Gases in Fluorocarbons*. Available at: http://detector-cooling.web.cern.ch/Detector-Cooling/data/Fluoro_Solubility.htm.
19. Heneghan AF, Haymet ADJ. Liquid-to-crystal nucleation: a new generation lag-time apparatus. *J Chem Phys*. 2002;117:5319–5327.
20. Maeda N, Wells D, Hartley PG, Kozielski KA. Statistical analysis of supercooling in fuel gas hydrate systems. *Energy Fuels*. 2012;26: 1820–1827.
21. Maeda N. Development of a high pressure electrical conductivity probe for experimental studies of gas hydrates in electrolytes. *Rev Sci Instrum*. 2013;84:015110.
22. Kashchiev D, Firoozabadi A. Nucleation of gas hydrates. *J Cryst Growth*. 2002;243:476–489.

Manuscript received Mar. 16, 2015, and revision received Apr. 29, 2015.